J Appl Electrochem (2010) 40:601–613
DOI 10.1007/s10800-009-0035-8

ORIGINAL PAPER

On the corrosion inhibition and adsorption behaviour of some benzotriazole derivatives during copper corrosion in nitric acid solutions: a combined experimental and theoretical study

K. F. Khaled · Mohamed A. Amin · N. A. Al-Mobarak

Received: 15 March 2009 / Accepted: 23 November 2009 / Published online: 10 December 2009

Abstract Copper corrosion inhibition in 1 M HNO_3 solution by some benzotriazole derivatives, namely *N*-(2-thiazolyl)-1H-benzotriazole-1-carbothioamide (TBC), *N*-(furan-2-ylmethyl)-1H-benzotriazole-1-carbothioamide (FBC) and *N*-benzyl-1H-benzotriazole-1-carbothioamide (BBC), was investigated by ac impedance, dc polarization and weight loss techniques. A significant decrease in the corrosion rate of copper was observed in presence of the investigated compounds. The corrosion rate was found to depend on the concentration and type of the inhibitor. The degree of surface coverage of the adsorbed inhibitor was determined by weight loss technique, and it was found that the results obeyed Langmuir adsorption isotherm. Tafel polarization data indicated that the three selected inhibitors were of mixed type. The reactivities of the compounds under investigation were analyzed through Fukui indices, derived from density functional theory (DFT), to explain their inhibition performance.

K. F. Khaled (✉)
Electrochemistry Research Laboratory, Chemistry Department, Faculty of Education, Ain Shams University, Roxy, Cairo 11711, Egypt
e-mail: khaledrice2003@yahoo.com

M. A. Amin
Chemistry Department, Faculty of Science, Ain Shams University, Abbssia, Cairo, Egypt

K. F. Khaled · M. A. Amin
Materials and Corrosion Laboratory, Faculty of Science, Taif University, Taif, Kingdom of Saudi Arabia

N. A. Al-Mobarak
Faculty of Education, Scientific sections, Girls Section, Chemistry Department, Princess Nora bint Abdulrahman University, Riyadh, Kingdom of Saudi Arabia

Keywords Acid corrosion inhibition · DFT · Quantum chemical calculations · Molecular dynamics simulations · Fukui indices

1 Introduction

Copper and its alloys are widely used in industry because of their excellent electrical and thermal conductivity and are often used in heating and cooling systems [1–3]. Several heterocyclic nitrogen containing compounds were used as corrosion inhibitors for copper in acidic media [4–11]. It reveals that most of these inhibitors were aromatic and heterocyclic compounds containing nitrogen. Benzotriazole (BTA) and its derivatives were studied extensively, and BTA was proved to be a highly efficient inhibitor for preventing copper and copper-base alloys corrosion in neutral and alkaline media [12–14].

Although BTA enables copper protection in various aqueous environments, its efficiency decreases dramatically in acid solutions and high temperature conditions [15–17]. It is generally accepted that its inhibition mechanism in neutral and alkaline solutions is the adsorption of single BTA molecules on the copper surface and the formation of a polymeric film of a (Cu^{+}BTA) complex [18]. However, in an acidic solution, BTA exists predominantly as a protonated species, $BTAH^{+}$. This protonated species is less strongly chemisorbed on the copper surface, as the metal is thought to be positively charged in acidic solution [15]. This in turn leads to a decrease in the inhibition efficiency of BTA in acidic solution.

There is a need for new inhibitors for copper corrosion in acidic media. A possible solution to this problem is to find new BTA derivatives that can act as efficient corrosion inhibitors in acid media. Recently, in our laboratory we

developed new benzotriazole derivatives that show better inhibition efficiency over BTA in acid medium for copper corrosion [19–21].

The aim of this study is to study the influence of three selected benzotriazole derivatives, namely *N*-(2-thiazolyl)-1H-benzotriazole-1-carbothioamide (TBC), *N*-(furan-2-ylmethyl)-1H-benzotriazole-1-carbothioamide (FBC) and *N*-benzyl-1H-benzotriazole-1-carbothioamide (BBC), on the corrosion of copper in 1 M HNO_3 solutions using experimental (chemical, electrochemical) and theoretical (quantum chemical molecular dynamics simulations) studies.

2 Experimental

The copper electrode used in this study is of 99.999% purity (Johnson Matthey Chemicals). The cylindrical copper rod was welded with iron-wire for electrical connection and mounted in Teflon with an active flat disc shaped surface of (0.28 cm^2) geometric area, to contact the test solution. Prior to each experiment, the copper electrode was polished with different grit sizes emery papers up to 4/0 grit size to remove the corrosion products if any formed on the surface. The copper electrode was etched in 7 M HNO_3 solution for 15 s, cleaned in 18 MΩ water in an ultrasonic bath for 5 min, and subsequently rinsed in acetone and bi-distilled water and immediately immersed in the test solution.

The benzotriazole derivatives are presented in Fig. 1. All of these compounds were obtained from Aldrich Chemical Co. They were put in 1 M HNO_3 (Fisher Scientific) without pre-treatment at concentrations of 10^{-4}, 5×10^{-4}, 10^{-3} and 5×10^{-3} M. The electrode was immersed in these solutions for 1 h before starting measurements; the time necessary to reach a quasi-stationary value for the open circuit potential.

A conventional electrochemical cell of capacity 250 ml was used. This cell contains three compartments for working, platinum mesh counter and reference electrodes. A Luggin-capillary was also included in the design, the tip of which was made very close to the surface of the copper electrode to minimize IR drop. The reference electrode was a saturated calomel (SCE) used directly in contact with the test solution. The measurements were carried out in aerated stagnant 1 M HNO_3 solutions at 25 °C (using water thermostat ±1 °C) without and with various concentrations (10^{-4} to 5×10^{-3} M) of benzotriazole derivatives, as possible corrosion inhibitors. All solutions were freshly prepared from analytical grade chemical reagents using doubly distilled water and were used without further purification. For each run, freshly prepared solutions as well as a cleaned set of electrodes were used.

Tafel polarization curves were obtained by changing the electrode potential automatically (from −280 to +200 mV_{SCE}) with a scan rate of 1 mV s^{-1}. Impedance measurements were carried out in a frequency range of 10 kHz to 20 mHz with an amplitude of 5 mV peak-to-peak using ac signals at open circuit potential. Measurements were performed with a Gamry Instrument Potentiostat/Galvanostat/ZRA. This includes a Gamry Framework system based on the ESA400, Gamry applications that include DC105

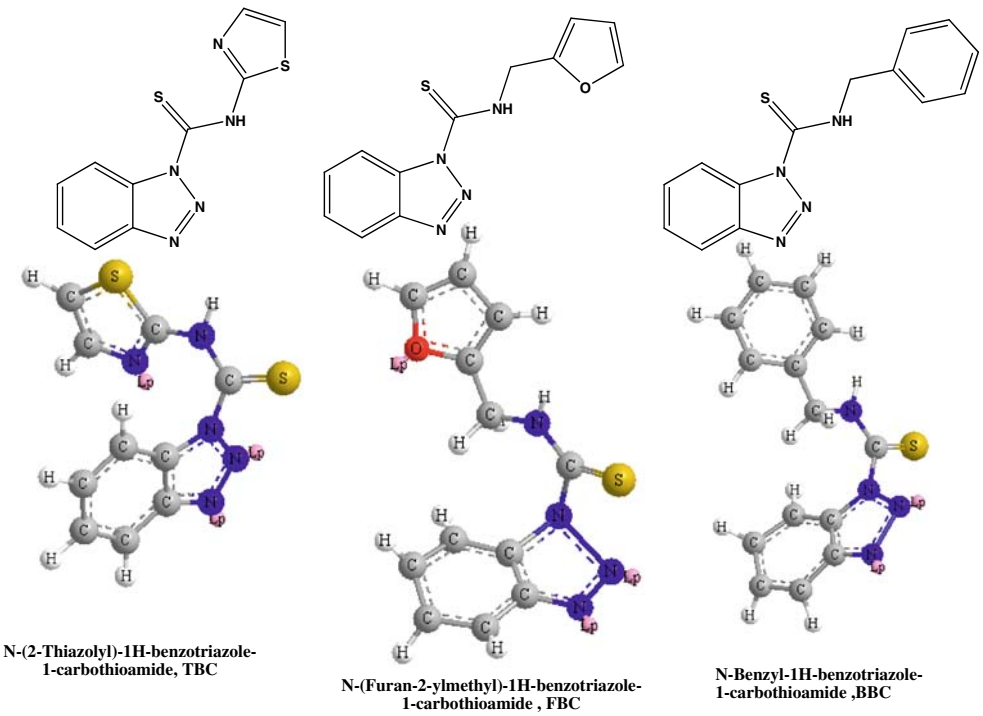

Fig. 1 Optimized structures of the studied benzotriazole derivatives calculated with DFT

for dc corrosion measurements, EIS300 for impedance measurements to calculate the corrosion current and the Tafel constants along with a computer for collecting the data. Echem Analyst 4.0 Software was used for plotting, graphing and fitting data.

The weight loss measurements were carried out in a 250 ml capacity glass beaker placed in a thermostat water bath. The solution volume was 100 ml. The used copper coupons (Puratronic, 99.999%) had a rectangular form (length = 2.5 cm, width = 2 cm, thickness = 0.05 cm). The coupons were weighed and suspended in a 100 ml of an aerated 1 M HNO_3 solution containing benzotriazole derivatives at the desired concentrations for 36 h exposure period of time at 25 ± 1 °C.

At the end of the tests, the coupons were taken out, washed with bidistilled water, degreased with acetone, washed again with bidistilled water, dried and then weighed using an analytical balance (precision: ± 0.1 mg). Three measurements were performed in each case and the mean value of the weight loss has been reported. The standard deviation of the observed weight loss was ± 1%. The corrosion rate, w, (expressed in mg cm^{-2} h^{-1}) as well as the inhibition efficiency (IE_w%) over the exposure time period were calculated according to the following equation:

$$IE_w\% = \left(1 - \frac{w}{w_o}\right) \times 100, \quad (1)$$

where w_o and w are the weight loss without and with benzotriazole derivatives, respectively.

3 Theory and computational details

In agreement with the DFT, the energy of the fundamental state of polyelectronic systems can be expressed through the total electronic density, and in fact the use of the electronic density instead of the wave function for the calculation of the energy constitutes the fundamental base of DFT [22].

The local reactivity of the molecules was analyzed through an evaluation of the Fukui indices (FI) [23]. These are a measurement of the chemical reactivity, as well as an indicative of the reactive regions and the nucleophilic and electrophilic behaviour of the molecule. The condensed Fukui functions [23] are found by taking the finite difference approximations from Mulliken population analysis of atoms in benzotriazole derivatives, depending on the direction of the electron transfer:

$$f_k^+ = q_k(N+1) - q_k(N) \quad \text{(for nucleophilic attack)}, \quad (2)$$

$$f_k^- = q_k(N) - q_k(N-1) \quad \text{(for electrophilic attack)}, \quad (3)$$

$$f_k^o = \frac{q_k(N+1) - q_k(N-1)}{2} \quad \text{(for radial attack)}, \quad (4)$$

where q_k is the gross charge of atom k in the molecule and N is the number of electrons.

The FI calculations were performed using Materials Studio [24, 25] $DMol^3$ version 4.3.1, a high quality quantum mechanics computer program (available from Accelrys, San Diego, CA). These calculations employed an ab initio, local density functional (LDF) method with a double numeric polarization (DNP) basis set and a Becke–Perdew (BP) functional. $Dmol^3$ use a Mulliken population analysis [26].

The molecular dynamics simulations procedures were used to calculate the interaction energy, $E_{Cu-inhibitor}$, of the Cu surface with the studied benzotriazole derivatives. The interaction energy was calculated according to Eq. 5:

$$E_{Cu-inhibitor} = E_{complex} - (E_{Cu} + E_{inhibitor}), \quad (5)$$

where $E_{complex}$ is the total energy of the Cu crystal together with the adsorbed inhibitor molecule, E_{Cu} and $E_{inhibitor}$ are the total energy of the copper crystal and free inhibitor molecular, respectively. The binding energy of the inhibitor molecule is the negative value of the interaction energy, $E_{biniding} = -E_{Cu-inhibition}$ [27]. The molecular dynamics simulations procedures were used and described elsewhere [27].

4 Results and discussions

4.1 Electrochemical measurements

4.1.1 Electrochemical impedance spectroscopy measurements

Figures 2, 3 and 4 show the Nyquist plots recorded for copper in 1 M HNO_3 solutions without and with various concentrations of TBC, FBC or BBC. Measurements were conducted at the respective corrosion potentials at 25 °C. At high-frequency values, the Nyquist plots present a depressed semicircle, whose diameter is a function of the concentration and the type of the introduced inhibitor. This high-frequency semicircle is attributed to the single time constant of charge-transfer resistance (R_{ct}) and the double-layer capacitance (C_{dl}) [28, 29]. In the high-frequency region, the electrode reaction is controlled by a charge-transfer process and the diameter of the semicircle represents the charge-transfer resistance (R_{ct}).

A long Warburg diffusion tail was observed at low frequency values. The tails are inclined at an angle of 45° to the real-axis at the very low frequencies; a diffusion controlled process is therefore exists. Studies reported in the literature [30], showed that the diffusion process is controlled by diffusion of dissolved oxygen from the bulk solution to the electrode surface. This diffusion tail still appears, even in presence of high concentrations of the

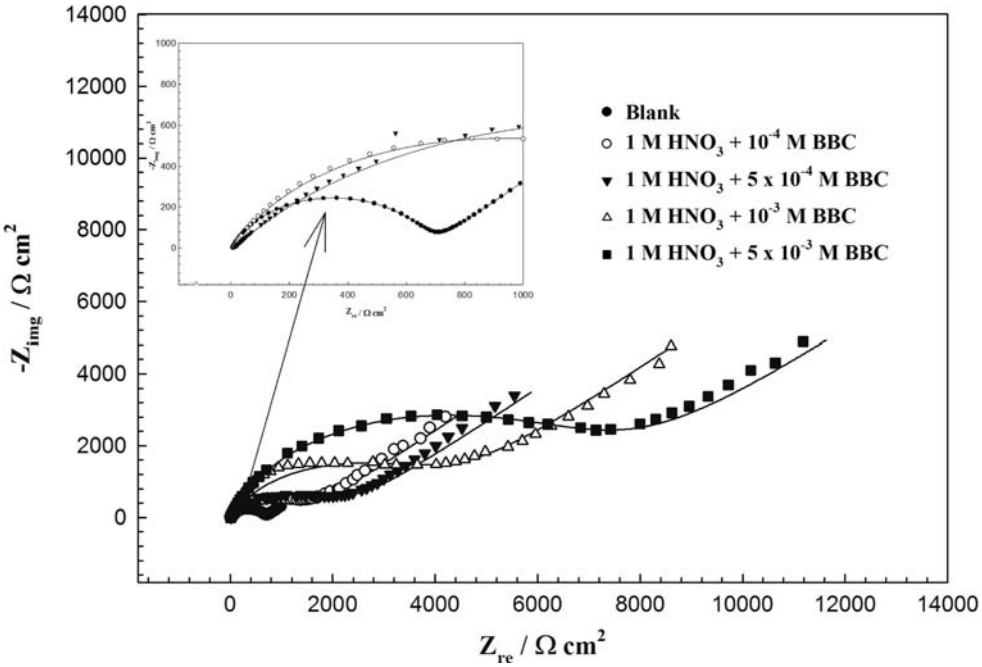

Fig. 2 Nyquist plots of a copper electrode in 1 M HNO_3 in the absence and presence of various concentrations of BBC at 25 ± 1 °C

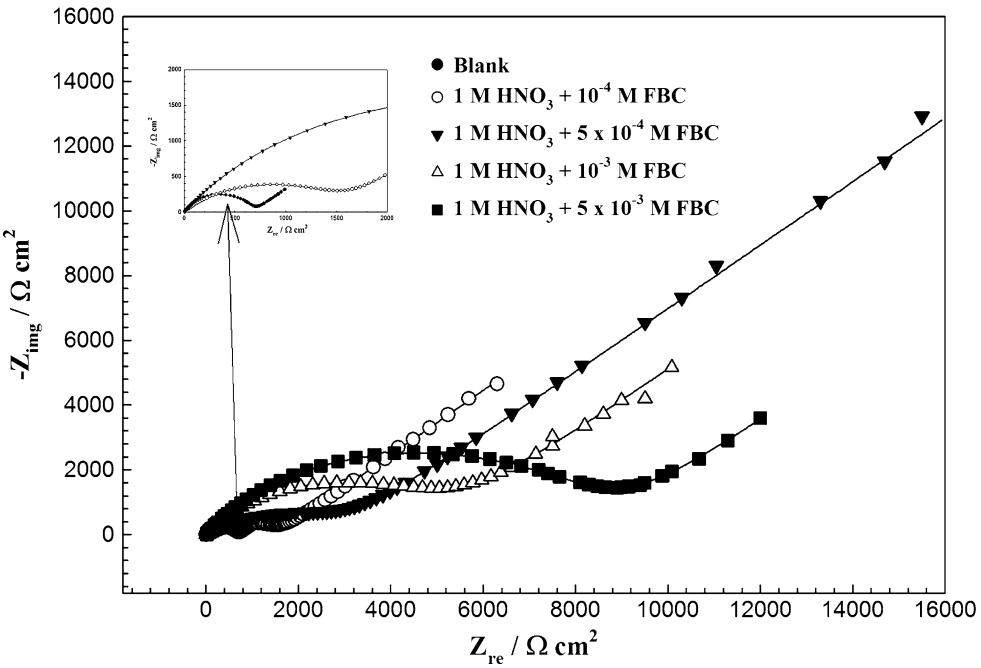

Fig. 3 Nyquist plots of a copper electrode in 1 M HNO_3 in the absence and presence of various concentrations of FBC at 25 ± 1 °C

tested inhibitors. This means that the corrosion behaviour of copper in the absence and presence of these inhibitors is influenced by mass transport. The increase of capacitive loop size with the addition of benzotriazole derivatives shows that a barrier gradually forms on the copper surface, protecting it from corrosion.

The equivalent circuit model, presented in Fig. 5, was successfully used to fit experimental impedance data. In Fig. 5, W stands for the Warburg impedance, R is a resistor (R_s = solution resistance and R_{ct} = charge-transfer resistance), and CPE represents the constant phase element. Here, CPE is substituted for double-layer capacitance, C_{dl}, to give a more accurate fit [31]. In most cases, the capacitive loops are depressed semicircles rather than regular ones, which are related to a phenomenon called the "dispersion effect." The admittance of CPE is described as:

$$Y_{CPE} = Y_o(j\omega)^n, \tag{6}$$

where j is the imaginary root, ω the angular frequency, Y_o the magnitude and n the exponential term [32].

Values of elements fitted with equivalent circuit in Fig. 5 are listed in Table 1. The percent inhibition

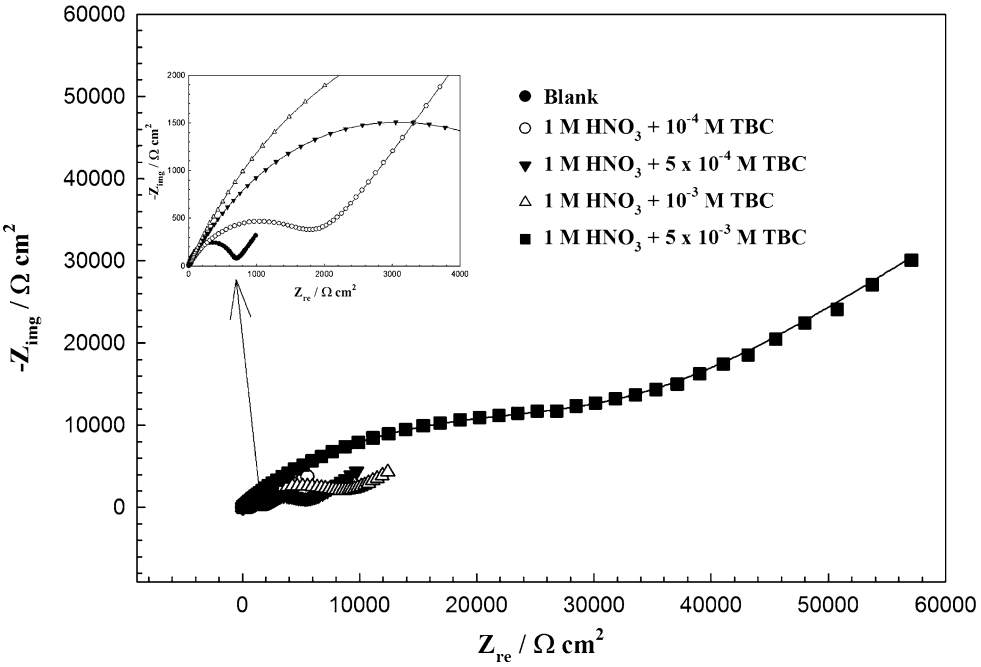

Fig. 4 Nyquist plots of a copper electrode in 1 M HNO_3 in the absence and presence of various concentrations of FBC at 25 ± 1 °C

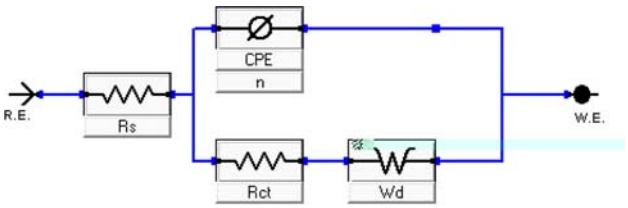

Fig. 5 Equivalent circuit model for the corrosion of copper displaying a Warburg impedance

efficiency values, see also Table 1, were calculated from the charge-transfer resistance values using Eq. 7:

$$\mathrm{IE}_i\% = \left(1 - \frac{R_{\mathrm{ct}}^{\mathrm{o}}}{R_{\mathrm{ct}}}\right) \times 100, \tag{7}$$

where $R_{\mathrm{ct}}^{\mathrm{o}}$ and R_{ct} are the charge-transfer resistances in the absence and the presence of benzotriazole derivatives, respectively. We remark that the value of inhibition efficiency increases with increase in benzotriazole derivatives concentrations up to 5×10^{-3} M reaching a maximum

Table 1 Impedance parameters extracted from the equivalent circuit presented in Fig. 5 for copper in 1 M HNO_3 in the absence and presence of various concentrations of BBC, FBC or TBC at 25 ± 1 °C

Concentration/M	$R_s/\Omega\ \mathrm{cm}^2$	CPE $\times\ 10^6/\mathrm{S\ s}^n$	n	$W_d \times 10^6/\mathrm{S\ s}^{1/2}$	$R_{\mathrm{ct}}/\Omega\ \mathrm{cm}^2$	$E_i\%$
Blank	5	30.3	0.79	900	675	
BBC						
10^{-4}	7	26.2	0.75	0.990	1449	53.421
5×10^{-4}	10	22.3	0.6	0.880	2258	70.11
10^{-3}	8	16.8	0.75	0.600	4018	83.20
5×10^{-3}	8	12.5	0.82	0.600	6888	90.20
FBC						
10^{-4}	4	22.5	0.55	0.600	1615	58.21
5×10^{-4}	2	19.3	0.43	0.200	3462	80.50
10^{-3}	2	14.1	0.65	0.550	5315	87.30
5×10^{-3}	6	10.2	0.65	0.850	8766	92.29
TBC						
10^{-4}	3	9.5	0.55	0.750	1940	65.21
5×10^{-4}	5	8.6	0.6	0.650	5672	88.09
10^{-3}	8	4.3	0.65	0.700	8766	92.29
5×10^{-3}	3	0.56	0.6	0.095	35530	98.10

value of 98.1% in case of TBC. These results suggest that TBC is the best inhibitor among the tested inhibitors.

4.1.2 Tafel polarization measurements

Polarization curves for copper electrode in 1 M HNO_3 at various concentrations of benzotriazole derivatives are shown in Figs. 6, 7 and 8. It shows, in all cases, that the presence of benzotriazole derivatives causes a prominent decrease in the corrosion rate, i.e. shifts the anodic curves to more positive potentials and the cathodic curves to more negative potentials, and to lower values of current densities. Namely, both cathodic and anodic reactions of copper electrode corrosion are inhibited by these inhibitors in 1 M HNO_3 solutions. This may be ascribed to adsorption of inhibitor over the corroded surface [33]. The values of corrosion current densities, i_{corr}, corrosion potential, E_{corr}, and

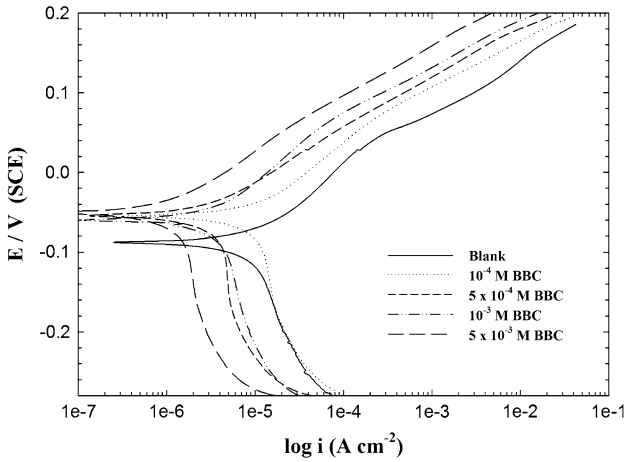

Fig. 6 Anodic and cathodic Tafel polarization curves for copper in 1 M HNO_3 in the absence and presence of various concentrations of BBC at 25 ± 1 °C

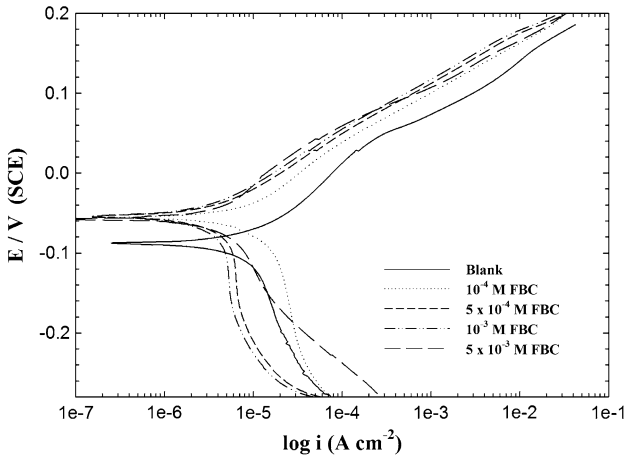

Fig. 7 Anodic and cathodic Tafel polarization curves for copper in 1 M HNO_3 in the absence and presence of various concentrations of FBC at 25 ± 1 °C

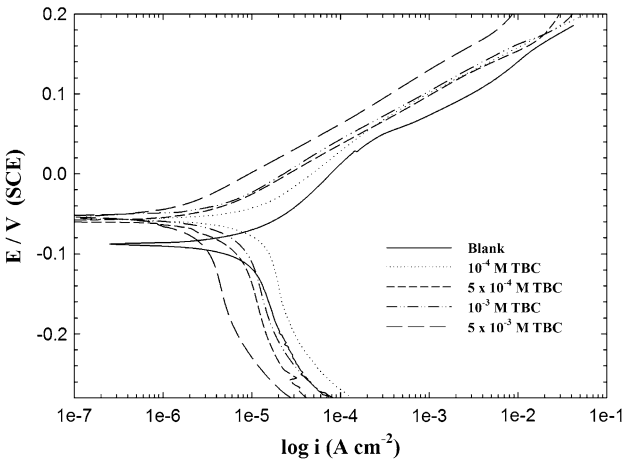

Fig. 8 Anodic and cathodic Tafel polarization curves for copper in 1 M HNO_3 in the absence and presence of various concentrations of TBC at 25 ± 1 °C

the cathodic (β_c) and anodic (β_a) Tafel slopes were calculated from the curves of Figs. 6–8, based on calculations presented in our previous study [21], as a function of the concentration of the three selected inhibitors. These electrochemical parameters, together with the inhibition efficiencies, IE_T(calculated from Eq. 8), are listed in Table 2

$$IE_T\% = \left(1 - \frac{i_{corr}}{i^o_{corr}}\right) \times 100, \quad (8)$$

where $i^o_{corr}$and i_{corr} are corrosion current densities in the absence and the presence of benzotriazole derivatives, respectively.

It follows from the data of Table 2 that the corrosion current, $i_{corr,}$ decreases, while IE_T enhances with increase in each inhibitor concentration. The maximum decrease in the corrosion current density was observed for the TBC derivative, corresponding to a maximum efficiency of about 93% at 5×10^{-3} M TBC, inspect Table 2. These results confirm impedance measurements that TBC is a better inhibitor than BBC and FBC. Further inspection of Table 2 reveals that the presence of these inhibitors does not remarkably shift the corrosion potential (E_{corr}), therefore, these three selected compounds can be described as mixed-type inhibitors for copper corrosion in 1 M HNO_3 solutions, and the inhibition of these compounds on copper is caused by geometric blocking effect, namely, the inhibition effect results from the reduction of the reaction area on the surface of the corroding copper [34].

Both the anodic and cathodic Tafel slopes slightly change upon addition of benzotriazole derivatives, see again Table 2. These findings mean that the inhibitor molecules are adsorbed on both the anodic and cathodic sites, retarding both anodic dissolution and cathodic reduction reactions. For copper corrosion in aerated acidic solutions at E_{corr}, the anodic reaction is copper dissolution

Table 2 Electrochemical kinetic parameters obtained by Tafel polarization technique for copper in 1 M HNO_3 in the absence and presence of various concentrations of BBC, FBC or TBC at 25 ± 1 °C

Concentration/M	i_{corr}/μA cm^{-2}	$-E_{corr}$/mV (SCE)	β_a/mV dec^{-1}	β_c/mV dec^{-1}	CR mmpy	E_T%
Blank	12.00	88.1	72.8	180.1	66.72e−3	000
BBC						
10^{-4}	6.34	54.4	71.3	237.4	73.88e−3	42.58
5×10^{-4}	2.64	54.0	66.7	295.1	30.72e−3	67.88
10^{-3}	2.26	59.1	74.1	219.7	26.30e−3	79.41
5×10^{-3}	0.943	50.6	70.2	270.1	11.02e−3	85.31
FBC						
10^{-4}	7.22	55.1	72.2	224.8	84.14e−3	53.57
5×10^{-4}	3.476	54.0	72.2	295.1	40.38e−3	73.82
10^{-3}	2.87	54.0	66.7	295.0	33.43e−3	83.11
5×10^{-3}	1.80	56.9	61.4	103.6	20.96e−3	89.32
TBC						
10^{-4}	7.79	57.2	72.1	210.4	90.79e−3	60.21
5×10^{-4}	4.06	58.8	65.4	231.2	47.12e−3	81.33
10^{-3}	3.37	55.3	63.4	182.2	39.32e−3	85.22
5×10^{-3}	2.03	53.3	68.8	242.4	23.64e−3	93.08

and cathodic reaction is oxygen reduction being the hydrogen discharge current density negligible as compared to oxygen reduction current density [35]. More details concerning the electrochemical reactions for copper in HNO_3 solutions are present in our previous study [36].

4.2 Weight loss measurements

Weight loss measurements were carried out in a 1 M HNO_3 free solution and in solutions containing different concentrations of benzotriazole derivatives. Corrosion rates of copper coupons, w, in (mg cm^{-2} h^{-1}) and the inhibition efficiency (IE_w) were calculated using Eq. 1. The average corrosion rates are shown in Table 3. The results show that all tested benzotriazole derivatives inhibited the corrosion of copper in 1 M HNO_3 solutions to an extend depending on concentration and type of the inhibitor introduced to the aggressive solution.

Increasing the concentration of each benzotriazole derivative increases the inhibition efficiency, IE_w. Maximum values of IE_wwere again recorded for TBC (97.4% at 5×10^{-3} M). The inhibition influence of these compounds against copper corrosion can be attributed to their adsorption on the copper surface, as will be seen, which limits the dissolution of the latter by blocking its corrosion sites. Rate of corrosion therefore decreases (corresponding to increased inhibition efficiency) with increase in inhibitor concentration.

4.3 Adsorption isotherms

To understand the mechanism of corrosion inhibition of copper in 1 M HNO_3 by the studied benzotriazole derivatives, the adsorption behaviour of these derivatives on the copper surface must be known. If simple adsorptive behaviour is assumed for these derivatives, a direct relationship between inhibition efficiency and surface coverage, θ, of the inhibitor will be existed. Weight loss data were used to evaluate the surface coverage values, based on Eq. 9 [37]:

$$\theta = \frac{w - w_o}{w_o}, \tag{9}$$

where w_o and w are weight loss values in the absence and presence of benzotriazole derivatives, respectively. The surface coverage values (θ) were tested graphically to allow fitting of a suitable adsorption isotherm. The plot of C/θ versus C, Fig. 9, yielded a straight line with a nearly unit slope. This result clearly proves that the adsorption of the benzotriazole derivatives from 1 M HNO_3 solution on the copper obeys the Langmuir adsorption isotherm, see Eq. 10:

$$\theta = \frac{KC}{KC + 1} \tag{10}$$

$$\frac{C_{inh}}{\theta} = \frac{1}{K} + C_{inh} \tag{11}$$

with

$$K = \left(\frac{1}{55.5}\right) \exp\left(-\frac{\Delta G_{ads}}{RT}\right), \tag{12}$$

where C_{inh} is the inhibitor concentration, θ is the fraction of the surface covered, K is the adsorption equilibrium constant and ΔG_{ads} is the standard free energy of adsorption. The value of 55.5 being the concentration of water in solution expressed in mole.

The values of K obtained from the Langmuir plot are about 7919, 12722 and 14191 for BBC, FBC and TBC,

Table 3 Corrosion rate (mg cm^{-2} h^{-1}) and the inhibition efficiency data obtained from weight loss measurements for copper in 1 M HNO_3 solutions without and with different concentrations of BBC, FBC or TBC at 25 ± 1 °C

Concentration/M	Corrosion rate/mg cm^{-2} h^{-1}	E_w%
Blank	0.341	–
BBC		
10^{-4}	0.163	52.2
5×10^{-4}	0.104	69.5
10^{-3}	0.062	81.8
5×10^{-3}	0.035	89.7
FBC		
10^{-4}	0.148	56.6
5×10^{-4}	0.069	79.7
10^{-3}	0.051	85.1
5×10^{-3}	0.032	90.6
TBC		
10^{-4}	0.126	63.1
5×10^{-4}	0.047	86.2
10^{-3}	0.030	91.2
5×10^{-3}	0.009	97.4

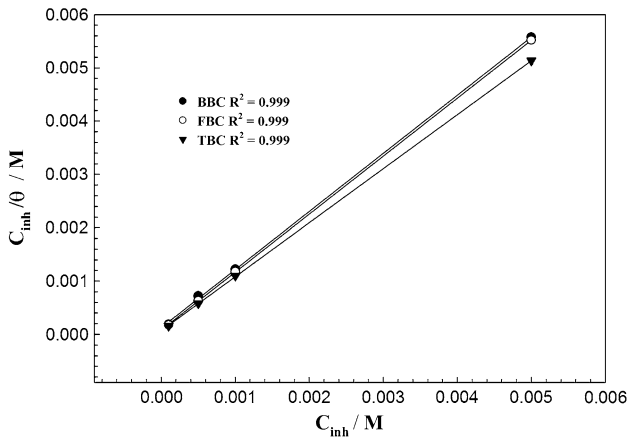

Fig. 9 Langmuir's isotherm for adsorption of benzotriazole derivatives in 1 M HNO_3 on the copper surface at 25 ± 1 °C

respectively. The values of ΔG_{ads} were calculated to be −32.1, −33.3 and −33.6 kJ mol^{-1} for BBC, FBC and TBC, respectively. The large negative value of ΔG_{ads} indicated that the studied benzotriazole derivatives were strongly adsorbed on the copper surface [38]. It is well known that the values of $-\Delta G_{ads}$ of the order of 20 kJ/mol or lower indicate a physisorption; those of order of 40 kJ/mol or higher involve charge sharing or a transfer from the inhibitor molecules to the metal surface to form a co-ordinate type of bond [39, 40]. On the other hand, Metikos-Hukovic et al. [41] described the interaction between thiourea and iron ($\Delta G_{ads} = -39$ kJ/mol) as chemisorption. The same conclusion was given by Wang et al. concerning the interaction between mercapto-triazole and mild steel ($\Delta G_{ads} = -32$ kJ/mol) [42]. Moreover, Bayoumi and Ghanem considered that the adsorption of naphthalene disulfonic acid on the mild steel was principally chemisorption ($\Delta G_{ads} = -28.47$ kJ/mol) [43].

The ΔG_{ads} values obtained here show that chemisorption of benzotriazole derivatives may occur. Benzotriazole derivatives were assumed to be adsorbed in the form of neutral molecules involving replacement of water molecules from the metal surface and sharing of electrons between the "N" and "S" atoms of the inhibitor molecule and copper surface. Adsorption of benzotriazole derivatives can also occur through π electron interactions between the benzotriazole ring structure of the molecule and the copper surface.

It was reported that the presence of benzotriazole derivatives induced the formation of semiconductive copper oxides [44]. This was possibly responsible for the improvement of corrosion resistance. The type of intermediates that formed on Cu surface in 1 M HNO_3 solution can be explained according to the potential-pH diagram of copper in HNO_3 solutions [21, 45]. It is seen that a stable Cu_2O is formed only in acidic solution of pH over 2. Nevertheless, since the proton H^+ is continuously consumed to the hydrogen gas during the Cu dissolution, the pH value near the Cu electrode in HNO_3 solution instantaneously jumps from 1 to greater values. Thus, it is acceptable to think that Cu_2O can be metastably formed on the Cu surface even at open circuit potential in nitric acid [8].

The presence of Cu_2O may facilitate adsorption via H-bond formation. Another possible mechanism, therefore may be adsorption assisted by hydrogen bond formation between protonated and unprotonated N atoms in the molecule and the oxidized surface (Cu_2O) species. The latter should be more prevalent for protonated N atoms, because the positive charge on N is conductive to the formation of hydrogen bonds. The extent of adsorption by the respective modes depends on the nature of the metal surface. The adsorption layer acts as an additional barrier to the corrosive attack and enhances the performance of the passive layer as a result.

A comparison of the inhibition performance of TBC with FBC and BBC showed, as previously proved here using chemical and electrochemical methods, that TBC was the most effective corrosion inhibitor among the three inhibitors used. These findings could be further explained on the basis that in the presence of dissolved oxygen, where the metal surface is oxidized, the ability of a benzotriazole derivative to provide corrosion inhibition is related to its tendency to form hydrogen bonds with the oxide species on the metal surface. Such capability should be proportional to the number of NH linkages in the molecule.

It is quite evident from the chemical structure of TBC molecule that it has, in addition to the benzotriazole

ring, thiazolyl and carbothioamide groups. These groups enhance its ability to adsorb strongly on copper surface. Also, increases the tendency to form hydrogen bonds with the oxidized surface. These results confirmed the importance of hydrogen bonding in effective corrosion inhibition in presence of oxide species. Due to this adsorption, inhibitor molecules block the reaction sites and reduce the rate of corrosion reaction [46].

4.4 Theoretical study

The optimized structures for the three inhibitors in their ground states are shown in Fig. 10. The frontier orbitals (highest occupied molecular orbital, HOMO) and (lowest unoccupied molecular orbital, LUMO) of a chemical species are very important in defining its reactivity. Fukui [47] first recognized this. A good correlation was found between

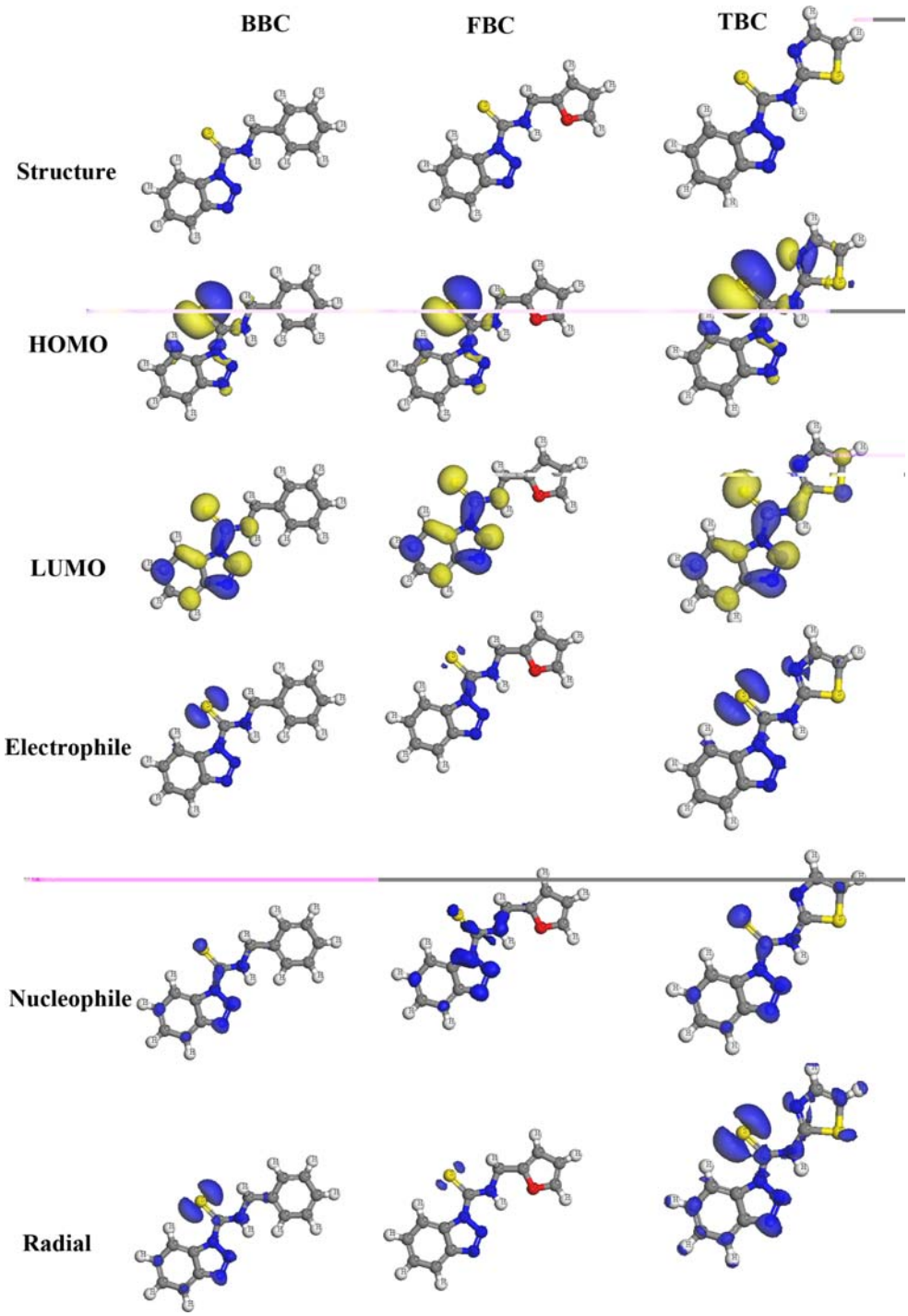

Fig. 10 Molecular orbital plots as well as active sites for electrophilic and nucleophilic attack on benzotriazole derivatives

the inhibition efficiency and E_{HOMO} which is often associated with the electron-donating ability of the molecule. The literature showed that the adsorption of the inhibitor on the metal surface can occur on the basis of donor–acceptor interactions between the π-electrons of the heterocyclic compound and the vacant orbitals of the metal surface atoms [48].

High values of E_{HOMO} reflect the tendency of the molecule to donate electrons to appropriate acceptor molecules with low energy, empty molecular orbitals. Thus, high values of E_{HOMO} facilitate adsorption, and hence the inhibition efficiency is enhanced. Similar relations were found between the inhibition efficiency and the energy gap $\Delta E = E_{LUMO} - E_{HOMO}$ [49, 50]. The energy of the lowest unoccupied molecular orbital indicates the ability of the molecule to accept electrons. The lower the value of E_{LUMO}, the more probable it is that the molecule would accept electrons. Lower values of the energy difference ΔE will render good inhibition efficiency, because the energy to remove an electron from the last occupied orbital will be low [51, 52].

The dipole moment μ is another way to obtain data on the electronic distribution in a molecule and is one of the properties more used traditionally to discuss and rationalize the structure and reactivity of many chemical systems [53]. In Table 4, certain quantum chemical parameters related to the molecular electronic structure are presented, such as: E_{HOMO}, E_{LUMO}, ΔE and μ. The values of E_{HOMO} show the relation TBC > FBC > BBC for this property. In addition, the values of the gap energy ΔE show the relation TBC < FBC < BBC for this property. The results for the calculations of the ionization potential (I) and the electron affinity (A) by application of Koopmans' theorem [49] are shown in Table 4. According to the Hartree–Fock theorem, the frontier orbital energies are given by: $-E_{HOMO} = I$, $-E_{LUMO} = A$.

This theorem establishes a relation between the energies of the HOMO and the LUMO and the ionization potential and the electron affinity, respectively. Although no formal proof of this theorem exists within DFT, its validity is generally accepted. For absolute electronegativity, χ, and global hardness, η, their operational and approximate definitions are $-\mu = (I + A)/2 = \chi$, $\eta = (I - A)/2$. Two systems, copper and inhibitor, are brought together, electrons will flow from lower χ (inhibitor) to higher χ (Cu), until the chemical potentials become equal. As a first approximation, the fraction of electrons transferred [54], ΔN, will be given by:

$$\Delta N = \frac{\chi_{Cu} - \chi_{inh}}{2(\eta_{Cu} + \eta_{inh})}, \tag{13}$$

where copper surface is the Lewis acid according to HSAB theory [55].

The difference in electronegativity drives the electron transfer, and the sum of the hardness parameters acts as a

Table 4 Quantum and molecular dynamics parameters derived for benzotriazole derivatives calculated with DFT method in aqueous phase

Total energy/ kcal mol^{-1}	HOMO/eV	LUMO/eV	ΔE/eV	μ/debye	$I = -E_{HOMO}$	$A = -E_{LUMO}$	$\chi = (I + A)/2$	$\eta = (I - A)/2$	$\Delta N = \frac{\chi_{Cu} - \chi_{inh}}{2(\eta_{Cu} + \eta_{inh})}$	$E_{Cu-inhibitor}$/ kcal mol^{-1}	$E_{binding}$ (kcal mol^{-1})
TBC											
−56990.8	−4.898	0.279	5.1770	1.407	4.898	−0.279	2.3095	2.5885	0.4193	−78.96	78.96
FBC											
−61684.1	−4.983	0.252	5.2350	1.846	4.983	−0.252	2.3655	2.6175	0.4039	−76.32	76.32
BBC											
−62267.9	−5.006	0.2477	5.2537	2.408	5.006	−0.2477	2.3792	2.6269	0.3999	−71.25	71.25

resistance [56]. In order to calculate the fraction of electrons transferred, a theoretical value for the absolute electronegativity of copper according to Pearson was used $\chi_{Cu} = 4.8$ eV [49], and a global hardness of $\eta_{Cu} = 0$, by assuming that for a metallic bulk $I = A$ [57] because they are softer than the neutral metallic atoms.

From Table 4, it is possible to observe that molecule TBC has a lower value of global hardness. The fraction of transferred electrons is also the largest for molecule TBC and, in turn, is FBC then BBC. The values of the interaction energy and the binding energy of the three benzotriazole derivatives on copper (110) surface are listed in Table 4. It is clear from Table 4 that the binding energy has a positive value. As the value of the binding energy increases, the more easily the inhibitor adsorbs on the metal surface, the higher the inhibition efficiency [27].

TBC has the highest binding energy comparing to FBC and BBC to the copper surface that found during the molecular dynamics simulation process described elsewhere [27]. High values of binding energy obtained with TBC molecules explain its highest inhibition efficiency from the theoretical point of view. Therefore, according to a series of properties calculated for each molecule shown in Table 4, the reactivity order, that is, the inhibitive effectiveness order for the molecules, are: TBC > FBC > BBC. The calculated results are in agreement with experimental results.

Table 5 shows Mulliken atomic charges calculated for the studied molecules. It is inferred that the more negative the atomic charges of the adsorbed centre, the more easily the atom donates its electrons to the unoccupied orbital of the metal. It is clear from Table 5 that nitrogen and sulphur atoms carrying negative charges centres which could offer electrons to the copper surface to form a coordinate-type of bond.

The local reactivity is analyzed by means of the condensed Fukui function; the condensed Fukui functions allow us to distinguish each part of the molecule on the basis of its distinct chemical behaviour due to the different substituent functional groups. Thus, the site for nucleophilic attack will be the place where the value of f_k^+ is a maximum. In turn, the site for electrophilic attack is controlled by the value of f_k^-. The values of the Fukui functions for a nucleophilic and electrophilic attack are given for the three inhibitors in Table 5 (only for the nitrogen, sulphur and oxygen atoms).

The FI values are presented in Table 5. TBC has propitious zones for electrophilic attack located on (N1, N2, N3, N11, S12 and S13), while FBC has only on (N1, N2, N3, N11, S12). BBC has only electrophilic centres on (N2 and S12). Data in Table 5 shows that TBC has more susceptible sites for adsorption on the copper surface, which again reflects its highest inhibition performance. The HOMO location on each system agrees with the atoms that exhibit greatest values of indices of Fukui (Fig. 10), both indicate the zones by which the molecule would be adsorbed on the copper surface (see Fig. 10).

The N values in Table 5 correspond to the number of electrons in the molecule. $N + 1$ corresponds to an anion, with an electron added to the LUMO of the neutral molecule. $N - 1$ correspondingly is the cation with an electron removed

Table 5 Calculated Mulliken atomic charges and Fukui functions for the three benzotriazole derivatives

Inhibitor	Atom	q_N	q_{N+1}	q_{N-1}	f_k^+	f_k^-	f_k^o
TBC	N(1)	−0.197	−0.198	−0.172	−0.001	−0.025	−0.013
	N(2)	−0.104	0.082	−0.117	0.186	0.013	0.050
	N(3)	−0.220	−0.027	−0.276	0.193	0.056	0.074
	N(11)	−0.538	−0.424	−0.552	0.114	0.014	0.014
	S(12)	−0.427	−0.137	−0.809	0.290	0.382	0.286
	S(13)	−0.181	−0.003	−0.290	0.178	0.109	0.093
	N(15)	−0.240	−0.128	−0.232	0.112	−0.008	0.002
FBC	N(1)	−0.198	−0.193	−0.178	0.005	−0.020	−0.007
	N(2)	−0.095	0.028	−0.108	0.123	0.013	0.063
	N(3)	−0.220	−0.105	−0.275	0.115	0.055	0.080
	N(11)	−0.522	−0.476	−0.550	0.046	0.028	0.032
	S(12)	−0.505	−0.320	−0.908	0.185	0.403	0.294
	O(14)	−0.378	−0.394	−0.333	−0.016	−0.045	−0.009
BBC	N(1)	−0.195	−0.189	−0.170	0.006	−0.025	−0.009
	N(2)	−0.104	−0.009	−0.123	0.113	0.019	0.066
	N(3)	−0.221	−0.117	−0.283	0.104	0.062	0.083
	N(11)	−0.530	−0.493	−0.569	0.037	0.039	0.038
	S(12)	−0.503	−0.321	−0.984	0.182	0.481	0.331

from the HOMO of the neutral. All calculations are done at the ground-state geometry. These functions can be condensed to the nuclei by using an atomic charge partitioning scheme, such as Mulliken population analysis in Eqs. 2–4.

An easy graphical display technique can also be used based on the Fukui functions. Instead of calculating the molecular orbitals for the neutral, cation and anion, we can just add or subtract electrons from the molecular orbitals of the neutral molecule. This procedure is not as good as described above, but it does give a quick graphical display of the susceptibility of different kinds of attack. So, rather than being a definitive calculation of a molecular property, freezing the molecular orbitals to those for the neutral molecule gives a useful graphical technique that can be rapidly applied.

5 Conclusions

Three selected benzotriazole derivatives, namely *N*-(2-thiazolyl)-1H-benzotriazole-1-carbothioamide, *N*-(furan-2-ylmethyl)-1H-benzotriazole-1-carbothioamide and *N*-benzyl-1H-benzotriazole-1-carbothioamide, were chemically and electrochemically investigated as corrosion inhibitors for copper in 1 M HNO_3 solution. Results obtained showed that:

- The inhibition efficiencies of the three selected benzotriazoles increased with increase in their concentrations.
- The three tested compounds were found to behave as mixed-type inhibitors.
- In impedance measurements, a depressed charge-transfer semicircle at high frequencies was observed followed by a well-defined Warburg diffusion the tail at low frequency values.
- The diameter of the depressed semicircle was a function of the concentration and the type of the inhibitor introduced to HNO_3 solution.
- Theoretical studies, made using the DFT method, were used to gain more information about the reactivity of the three benzotriazole derivatives as corrosion inhibitors.
- Calculations of the HOMO, the energy gap ΔE and the fraction of transferred electrons ΔN demonstrated that the order of the inhibitive effectiveness of these compounds follows the sequence: TBC > FBC > BBC, and this agrees well with experimental results.
- Reactive sites for nucleophilic and electrophilic attacks were indicated using the Fukui functions.
- For the nucleophilic and electrophilic attacks, reactive sites of the three studied inhibitors are located on the benzotriazole ring.
- TBC is unique in containing a thiazole ring which enhances its adsorption on copper surface.

References

1. Stupnisek-Lisac E, Bozic AL, Cafuk I (1998) Corrosion 54:713
2. Gasparac R, Martin CR, Stupnisek-Lisac E (2000) J Electrochem Soc 147:548
3. Zaky AM (2001) Br Corros J 36:59
4. Ling Y, Guan Y, Han KN (1995) Corrosion 51:367
5. Zucchi F, Trabanelli G, Monticelli C (1996) Corros Sci 38:147
6. Chen JH, Lin ZC, Chen S, Nie LH, Yao SZ (1998) Electrochim Acta 43:265
7. Marconato JC, Bulhoes LO, Temperini ML (1998) Electrochim Acta 43:771
8. Lee WJ (2003) Mat Sci Eng A348:217
9. Mihit M, Salghi R, El Issami S, Bazzi L, Hammouti B, Addi EA, Kertit S (2006) Pigment Resin Technol 35:151
10. El-Naggar MM (2000) Corros Sci 42:773
11. Fouda AS, Abd El-Aal A, Kandil AB (2006) Desalination 201:216
12. Musiani MM, Mengoli G (1987) J Electroanal Chem 217:187202
13. Da Costa SFLA, Agostinho SML, Rubim JC (1990) J Electroanal Chem 295:203
14. Brusic V, Frisch MA, Eldridge BN, Novak FP, Kauman FB, Rush BM, Frankel GS (1991) J Electrochem Soc 138:2253
15. Wu YC, Zhang P, Pickering HW, Ahara DL (1993) J Electrochem Soc 140:2791
16. Penninger J, Woppermann K, Schultze JW (1987) Werkst Korros 38:649
17. Hope GA, Davis CA, Schweinsberg DP (1994) In: Proceeding of ninth Australasian electrochemistry conference, Part I, 07-1, University of Wollongong, Wollongong, NSW, Australia
18. El-Taib F, Haruyama S (1980) Corros Sci 20:887
19. Khaled KF (2009) Electrochim Acta 54:4345–4352
20. Khaled KF, Fadllalh S, Hammouti B (2009) Mater Chem Phys 117:148–155
21. Khaled KF, Amin AM (2009) Corros Sci 51:2098–2106
22. Andrés J, Beltran J (2000) Química Teórica y Computacional. Universitat Jaume I, Castellón de la Plana, España
23. Yang W, Mortier WJ (1986) J Am Chem Soc 108:5708
24. Delley B (1990) J Chem Phys 92:508
25. Delley B (2000) J Chem Phys 113:7756
26. Mulliken RS (1995) J Chem Phys 23:1833
27. Khaled KF (2009) J Solid State Electrochem 13:1743–1756
28. Barcia OE, Mattos OR, Pebere N, Tribollet B (1993) J Electrochem Soc 140:2825
29. Feng Y, Teo WK, Siow KS, Tan KL, Hsieh AK (1996) Corros Sci 38:369
30. Ma H, Chen S, Niu L, Zhao S, Li S, Li D (2002) J Appl Electrochem 32:65
31. Wu X, Ma H, Chen S, Xu Z, Sui A (1999) J Electrochem Soc 146:1847
32. Benedetti AV, Sumodjo PTA, Nobe K, Cabot PL, Proud WG (1995) Electrochim Acta 40:2657
33. Mu GN, Li XH, Qu Q, Zhou J (2006) Corros Sci 48:445
34. Li X, Deng S, Fu H, Li T (2009) Electrochim Acta 54:89
35. Smyrl WH (1981) Electrochemistry and corrosion on homogeneous and heterogeneous metal surface. In: Bockris JO'M, Conway B, Yager E, White RE (eds) Comprehensive treatise of electrochemistry, vol 4. Plenum Press, New York, London, 97 pp
36. Khaled KF (2008) Mater Chem Phys 112:104–111
37. Zvauya R, Dawson JL (1994) J Appl Electrochem 24:943
38. Cano E, Polo JL, Iglesia AL, Bastidas JM (2004) Adsorption 10:219
39. Li XH, Mu GN (2005) Appl Surf Sci 252:1254
40. Li GM (2003) Anti-Corros Methods Mater 50:410
41. Li XH, Deng SD, Fu H, Mu GN (2008) Corros Sci 50:2635

42. Bensajjay E, Alehyen S, Achouri ME, Kertit S (2003) Anti-Corros Methods Mater 50:402
43. Bentiss F, Lebrini M, Lagrenée M (2005) Corros Sci 47:2915
44. Thomas JGN (1980) In: Proceedings of 5th European symposium on corrosion inhibitors, Ann. Univ. Ferrara, Italy, 453 pp
45. Pourbaix M (1975) Atlas of electrochemical equilibria in aqueous solutions. NACE, Houston, TX
46. Sahin M, Bilgic S, Yilmaz H (2002) Appl Surf Sci 195:1
47. Ignaczak A, Gomes JANF (1996) Chem Phys Lett 257:609
48. Hackerman N, Snavely E Jr, Payne JS Jr (1966) J Appl Electrochem 113:677–681
49. Sastri VS, Perumareddi JR (1997) Corros Sci 53:617–622
50. Ögretir C, Mihçi B, Bereket G (1999) J Mol Struct 488:223–231
51. Khalil N (2003) Electrochim Acta 48:2635–2640
52. Lukovits I, Pálfi K, Bakó I, Kálmán E (1997) Corrosion 53:915–919
53. Sastri VS (1998) Corrosion inhibitors: principles and applications. Wiley, Chichester, England
54. Wang He, Wang X, Wang Ha, Wang L, Liu A (2007) J Mol Modeling 13:147
55. Pearson RG (1988) Inorg Chem 27:734–740
56. Pearson RG (1963) J Am Chem Soc 85:3533–3539
57. Valdez R, Martinez-Villafane LM, Glossman-Mitnik D (2005) J Mol Struct 716:61